Ocean Dynamics (2022) 72:241–257
https://doi.org/10.1007/s10236-022-01503-1

Stability analysis of finite amplitude interfacial waves in a two-layer fluid in the presence of depth uniform current

Tanmoy Pal[1] · Asoke Kumar Dhar[1]

Received: 29 August 2021 / Accepted: 24 February 2022 / Published online: 4 March 2022

Abstract
A fourth-order nonlinear evolution equation of interfacial progressive waves in two-layer fluids of finite depths is derived in the case when there is a depth uniform current in the lower fluid. Based on this equation, stability analysis is then determined of a plane progressive wave. Discourses are provided for both air–water interface and a Boussinesq approximation. Graphs are plotted for maximum growth rate of instability as a function of wave steepness. Two-dimensional instability regions in the perturbed wavenumber plane and three-dimensional contour plots of growth rate of instability are also drawn. Starting from third-order nonlinear Schrödinger equation in one spatial dimension, we have additionally found the effect of depth uniform current on Peregrine breather. The present fourth-order analysis shows significant deviation from the third-order analysis and produces results consistent with the exact numerical results.

Keywords Nonlinear evolution equation · Interfacial gravity waves · Stability analysis · Peregrine breather

1 Introduction

The stability of progressive Stokes waves on the surface of infinite and finite depths of water has been analyzed numerically by McLean et al. (1981) and McLean (1982a, b). These studies reveal that there is an infinite hierarchy of type I and type II instabilities, starting from the centre with type I, the next outwards being type II, then the next is type I, and then again type II and so forth. The criterion to distinguish these two types of instability is the point of symmetry of the instability pattern. Later on, Yuen (1984) has extended the analysis of McLean et al. (1981) for interfacial gravity waves with a basic current jump across the interface and he has studied the stability analysis when the two fluids are infinitely deep. Grimshaw and Pullin (1985) have also derived a cubic nonlinear Schrödinger equation coupled to a wave induced mean flow equation for two superposed fluids of finite depths to study slowly modulated waves and have investigated the two-dimensional instability as a special case of long wavelength perturbation and small wave steepness. In the next paper, Grimshaw and Pullin (1985) have complemented their analytical results with numerical results for the stability of finite amplitude waves. As waves nearly always coexist with currents in an ocean and currents can significantly alter the characteristics of gravity waves [(Longuet and Stewart 1961; Bretherton and Garrett 1968; Peregrine 1976; Kantardgi 1995)], therefore nonlinear wave-current interactions call attention to scientists in ocean engineering and fluid dynamics. Sufficiently large waves can be generated in the areas when there are strong currents and particularly for waves which move against currents. Furthermore, in these situations, freak waves have been often formed [(Onorato et al. 2011; Ruban 2012; Toffoli et al. 2013)]. It is known that the interactions between waves and currents mainly rely on the direction of propagation of waves and the vertical distribution of currents [(Peregrine 1976; Liu et al. 1990; Huang and Mei 2003)]. Liao et al. (2017) have derived a cubic nonlinear Schrödinger equation for gravity waves in finite depth of water for the case when the combined effects of depth-uniform currents and constant vorticity are considered. However, research carrying on wave-current interactions has often assumed that currents are uniform with depth

Responsible Editor: Amin Chabchoub

✉ Asoke Kumar Dhar
asoke.dhar@gmail.com

Tanmoy Pal
tpal2966@gmail.com

[1] Department of Mathematics, Indian Institute of Engineering Science and Technology, Shibpur 711103, West Bengal, India

[(Toffoli et al. 2013, 2015; Stocker and Peregrine 1999)], that is to say, they are not vertically sheared. Toffoli et al. (Toffoli et al. 2013) have showed experimentally that a stable wave moving into a region characterized by an opposite uniform current U_0 may become modulationally unstable. From a physical point of view, they have also remarked that the process which they have analyzed may take place in nature when a modulationally stable swell, which is characterized by a narrow spectrum, enters a region of an opposing variable current. Again there are some circumstances for which currents are not uniform with depth (namely, they are vertically sheared) as in the cases of currents due to wind flow and ebb stream at a river mouth [(Mei and Lo 1984; Maciver et al. 2006)]. Furthermore, Hjelmervik and Trulsen (2009) have derived a current modified cubic nonlinear Schrödinger equation which allows a small amount of vorticity and investigated the influence of nonlinearity with respect to the variation of significant wave height, kurtosis, and occurrence of rogue waves. They have observed that the largest number of rogue waves on an opposing current jet is generated at the jet sides where the significant wave height is small. Considering the importance of currents in the water, Turpin et al. (1983) have investigated a nonlinear Schrödinger equation which covers the influence of currents and varying depth. From their analysis, it is found that the following current has a stabilizing influence on a wave train while the opposing current has the reverse effect. Later on, a current modified nonlinear evolution equation has been derived by Gerber (1987). In that paper, he has argued that opposing currents increase the growth rate of instability and also spread out the onset criterion. Effects reverse to these are observed in the case of the following currents. Again, an extension to the analysis of Dysthe (1979) to consider the influence of depth uniform currents is made by Stocker and Peregrine (1999).

All those studies have made from a lowest order (i.e., third-order) nonlinear Schrödinger equation by the said authors. Dysthe (1979) has pointed out that a notable improvement can be achieved by considering the perturbation analysis one step further, that is, adding fourth-order terms in the cubic Schrödinger equation, and he has derived a fourth-order nonlinear evolution equation for application to deep water gravity waves. Later on, Dhar and Das (1990) have extended the analysis of Dysthe (1979) in the presence of wind flowing over water. So that paper considered the effect of wind on Benjamin-Feir instability. Based on the fourth-order evolution equation, the expressions of the maximum growth rate of instability and the frequency at marginal stability are obtained, and graphs are plotted for those two expressions as a function of wave steepness. Furthermore, Dhar and Das (1994) have studied analytically the stability analysis from fourth-order nonlinear evolution equation for interfacial gravity waves when there is a basic current shear in both of the fluids of infinite depths. They have plotted the graphs for maximum growth rate of instability and for wavenumber at marginal stability as a function of wave steepness in the case of air–water interface. In the case of Boussinesq approximation, they have compared their fourth-order results with the exact numerical results of Pullin and Grimshaw (1986), and they are showed to agree fairly well. Considering the importance of the fourth-order evolution equation, in the present paper, we have developed a nonlinear evolution equation correct to fourth-order in wave steepness for interfacial progressive waves in two-layer finite depth fluids for the case when there is a depth uniform current in the lower fluid. On the basis of this equation, stability analysis is then made both for finite and infinite depths of fluids for a uniform wave train. Graphs are plotted for maximum growth rate of instability as a function of wave steepness for finite and infinite depths of fluids and for some values of depth uniform current v corresponding to both air–water and Boussinesq approximation. Two-dimensional instability regions are drawn for infinite depths of fluids for several values of v and wave steepness α_0 corresponding to air–water interface ($r = 0.00129$), Boussinesq approximation ($r \to 1$), $r = 0.1, 0.9$, and an important case for $r = 0$ for water waves. The latter three cases are then compared to the exact numerical results obtained by Yuen (1984) and McLean et al. (1981), and it is found from the figures that fourth-order equation gives better results which are closer to the exact numerical results obtained by them. We have also drawn some contour plots of growth rate of instability in the perturbed wavenumbers plane. Moreover, the effect of depth uniform current on Peregrine breather has been investigated by considering the third-order nonlinear Schrödinger equation in one space variable. Therefore, the present study extends the analysis of Grimshaw and Pullin (1985) to fourth order in a parameter ϵ representing the wave steepness in the presence of uniform current in the lower fluid.

2 Basic equations and assumption

We take $z = \zeta(x, y, t)$ as the equation of the common interface of two inviscid, irrotational, and incompressible fluids. The two fluids of densities ρ and ρ' are bounded by two horizontal planes at $z = d_1$ and $z = -d_2$. The basic unperturbed flow has a uniform velocity v towards x-direction in the lower layer, $-d_2 \le z \le 0$. It is found useful to consider dimensionless variables that are introduced by the following transformations

$$\left(\frac{k_0^3}{g}\right)^{\frac{1}{2}}(\phi, \phi') \to (\phi, \phi'),\ k_0(x, y, z, \zeta, d_1, d_2) \to (x, y, z, \zeta, d_1, d_2),$$
$$\omega t \to t, \left(\frac{k_0}{g}\right)^{\frac{1}{2}} v \to v, r = \frac{\rho'}{\rho}. \tag{1}$$

For describing the interfacial waves, we consider the governing equations as follows

$$\nabla^2\phi' = 0, \text{in } \zeta < z < d_1 \quad (2)$$

$$\nabla^2\phi = 0, \text{in } -d_2 < z < \zeta \quad (3)$$

$$\phi'_z - \zeta_t = \phi'_x\zeta_x + \phi'_y\zeta_y, \text{when } z = \zeta \quad (4)$$

$$\phi_z - \zeta_t - v\zeta_x = \phi_x\zeta_x + \phi_y\zeta_y, \text{when } z = \zeta \quad (5)$$

$$\phi_t - r\phi'_t + v\phi_x + (1-r)\zeta = -\tfrac{1}{2}(\nabla\phi)^2 + \tfrac{r}{2}(\nabla\phi')^2, \text{when } z = \zeta \quad (6)$$

$$\phi'_z = 0, \text{on } z = d_1 \quad (7)$$

$$\phi_z = 0, \text{on } z = -d_2. \quad (8)$$

We take the solutions of the above equations given by

$$Q = Q_0 + \sum_{n=1}^{\infty}\left[Q_n \exp\{in(kx + ly - \omega t)\} + \text{c.c.}\right], \quad (9)$$

in which Q symbolizes for ϕ, ϕ', ζ, (k, l) represents the wavenumber vector, $k_0 = \sqrt{k^2 + l^2}$, and c.c. represents complex conjugate. Here $\phi_0, \phi'_0, \phi_n, \phi'_n (n = 1, 2)$ and their complex conjugates are functions of a time scale $t_1 = \epsilon t$, a space scale $(x_1, y_1) = \epsilon(x, y)$ and z. $\zeta_0, \zeta_n, \zeta^*_n (n = 1, 2)$ are slowly varying functions of x_1, y_1, t_1. ϵ is a small ordering parameter measuring the weakness of nonlinearity, where $0 < \epsilon << 1$.

Subsequently, we assume that the wave is moving along the direction of x and so we put $l = 0$. The frequency ω and wavenumber k of the basic wave satisfy the following linear dispersion relation

$$f(\omega, k) \equiv (\omega - kv)^2\sigma_1 + r\sigma_2\omega^2 - (1-r)\sigma_1\sigma_2 k = 0, \quad (10)$$

where $\sigma_i = \tanh kd_i, i = (1, 2)$.

We now suppose that the first harmonic linear wave, whose nonlinear evolution equation we are going to study, has its wavenumber equal to the characteristic wavenumber k_0. Therefore, we have $k = 1$ and the relation (10) for finding ω becomes

$$(\sigma_1 + r\sigma_2)\omega^2 - 2\sigma_1 v\omega + \sigma_1 v^2 - (1-r)\sigma_1\sigma_2 = 0. \quad (11)$$

Equation (11) yields two values of ω given by

$$\omega_{\pm} = \frac{\sigma_1 v \pm \sqrt{\sigma_1\sigma_2[(1-r)(\sigma_1 + r\sigma_2) - rv^2]}}{(\sigma_1 + r\sigma_2)} \quad (12)$$

that corresponds to two modes and we specify these as positive and negative modes. The positive mode propagates along the positive direction of the x-axis with a frequency $[\sigma_1 v + \sqrt{\sigma_1\sigma_2\{(1-r)(\sigma_1 + r\sigma_2) - rv^2\}}]/(\sigma_1 + r\sigma_2)$, whereas the other mode propagates in the negative direction of the x-axis with a frequency $[\sqrt{\sigma_1\sigma_2\{(1-r)(\sigma_1 + r\sigma_2) - rv^2\}} - \sigma_1 v]/(\sigma_1 + r\sigma_2)$, provided $\sqrt{\sigma_1\sigma_2\{(1-r)(\sigma_1 + r\sigma_2) - rv^2\}} > \sigma_1 v$. The linear stability analysis is invariant under the transformation v into $-v$. Therefore, the results due to negative mode can be achieved from the results due to positive mode by changing v to $-v$.

Equation (12) corresponds to Kelvin–Helmholtz modes. When the heavier fluid is under the lighter one and the two fluids are at rest relative to each other, the plane interface is stable and supports gravity waves. Again, in the presence of depth uniform current v, the plane interface becomes unstable to disturbances of sufficiently short wavelengths. From (12), it follows that the plane surface is unstable if

$$v^2 > [\frac{(1-r)(\sigma_1 + r\sigma_2)}{r}],$$

which is known as the classical Kelvin–Helmholtz instability.

For linear stability, we get from (12), the following condition

$$|v| < [\frac{(1-r)(\sigma_1 + r\sigma_2)}{r}]^{\frac{1}{2}}.$$

So our analysis will remain valid as long as the nondimensional velocity of the lower fluid becomes less than the critical value $|v_c| = [\frac{(1-r)(\sigma_1+r\sigma_2)}{r}]^{\frac{1}{2}}$. For infinite depths of fluids, $\sigma_1 = \sigma_2 = 1$, and for air–water interface, $r = 0.00129$; hence, v_c becomes 27.8423. Now, ϕ_n, ϕ'_n, and ζ_n are the perturbed quantities and so we have considered the perturbation expansions (17) of them using the ordering parameter ϵ, whereas v and r are not the perturbed quantities. Therefore, the small value $r = 0.00129$ and the large value $v = 27.8423$ will not affect the ordering of the terms in the nonlinear analysis (see Dhar and Das (1990) and Senapati et al. (2016)).

The group velocity c_g of the basic wave is found from dispersion relation

$$c_g = \{(1-r)(\delta_1 + \sigma_1\sigma_2) - \delta_2\omega^2 + 2\delta_3\omega v - (\sigma_1 + \delta_3)v^2\}\{2(\sigma_1 + r\sigma_2)\omega - 2\sigma_1 v\}^{-1}, \quad (13)$$

where
$$\delta_1 = \sigma_1 d_2(1 - \sigma_2^2) + \sigma_2 d_1(1 - \sigma_1^2),$$
$$\delta_2 = d_1(1 - \sigma_1^2) + rd_2(1 - \sigma_2^2),$$
$$\delta_3 = \sigma_1 + d_1(1 - \sigma_1^2).$$

3 Derivation of evolution equation for interfacial gravity waves

Substituting the expression (9) in (2) and (3), we get the solutions for $\phi'_n, \phi_n (n = 1, 2)$ given by

$$\phi_n' = \frac{\cosh[(z-d_1)\Delta_n]}{\cosh d_1\Delta_n}A_n', \quad \phi_n = \frac{\cosh[(z+d_2)\Delta_n]}{\cosh d_2\Delta_n}A_n, \tag{14}$$

and ϕ_0', ϕ_0 as

$$\overline{\phi}_0' = \frac{\cosh[(z-d_1)\epsilon\overline{k}]}{\cosh\epsilon\overline{k}d_1}A_0', \quad \overline{\phi}_0 = \frac{\cosh[(z+d_2)\epsilon\overline{k}]}{\cosh\epsilon\overline{k}d_2}A_0, \tag{15}$$

where A_n' and A_n $(n = 1, 2)$ are the functions of x_1, y_1, t_1, and $\Delta_n = [(n - i\epsilon\frac{\partial}{\partial x_1})^2 - \epsilon^2\frac{\partial^2}{\partial y_1^2}]^{\frac{1}{2}}$. Here, $\overline{\phi}_0', \overline{\phi}_0$ are Fourier transforms of ϕ_0', ϕ_0, respectively, defined by

$$\left(\overline{\phi}_0', \overline{\phi}_0\right) = \iiint_{-\infty}^{\infty} \left(\overline{\phi}_0', \phi_0\right) \exp\left[-i\left(\overline{k}_x x_1 + \overline{k}_y y_1 - \overline{\omega} t_1\right)\right] \mathrm{d}x_1 \mathrm{d}y_1 \mathrm{d}t_1, \tag{16}$$

in which $\overline{k}^2 = \overline{k}_x^2 + \overline{k}_y^2$ and A_0', A_0 are functions of $\overline{k}_x, \overline{k}_y$, and $\overline{\omega}$.

We now take the following perturbation expansions for solving three sets of equations corresponding to $n = 0, 1, 2$

$$B_m = \sum_{n=1}^{\infty} \epsilon^n B_{mn}, (m = 0, 1), B_2 = \sum_{n=2}^{\infty} \epsilon^n B_{2n}, \tag{17}$$

in which B_j symbolizes for A_j', A_j, and $\zeta_j (j = 0, 1, 2)$.

Substituting (17) in the Taylor's expanded form of Eqs. (4) to (6) about $z = 0$ and then equating coefficients of $\exp in(x - \omega t)$ for $n = 1, 2, 0$ on both sides, we obtain a sequence of equations. From Eqs. (4) and (5) for $n = 1$ corresponding to first set, we obtain solutions of A_{11}', A_{12}' and A_{11}, A_{12} respectively. Next from Eqs. (4), (5), and (6) for $n = 2$ and 0 corresponding to second and third sets, we obtain solutions of $A_{22}', A_{23}', A_{22}, A_{23}, \zeta_{22}, \zeta_{23}$ and $A_{01}', A_{02}', A_{01}, A_{02}, \zeta_{01}, \zeta_{02}$ respectively. In the end, the equation resulting from (6) of the first set of equations can be expressed in the following form

$$f(\omega_1, k_1, l_1)\zeta_1 = -ir\sigma_2\omega_1 a_1 - i\sigma_1(\omega_1 - k_1 v)b_1 - \sigma_1\sigma_2\Delta_1 c_1, \tag{18}$$

where $\omega_1 = \omega + i\epsilon\frac{\partial}{\partial t_1}, k_1 = 1 - i\epsilon\frac{\partial}{\partial x_1}, l_1 = -i\epsilon\frac{\partial}{\partial y_1}$, and a_1, b_1, c_1 are contributions from nonlinear terms.

Inserting solutions of different quantities arising on the right side of (18), applying the transformations

$$\xi = x_1 - c_g t_1, \eta = y_1, \tau = \epsilon t_1 \tag{19}$$

and finally setting $\zeta = \zeta_1 = \zeta_{11} + \epsilon\zeta_{12}$, we obtain the fourth-order nonlinear evolution equation as follows

$$\begin{aligned} &i\frac{\partial\zeta}{\partial\tau} - \gamma_1\frac{\partial^2\zeta}{\partial\xi^2} + \gamma_2\frac{\partial^2\zeta}{\partial\eta^2} + i\gamma_3\frac{\partial^3\zeta}{\partial\xi^3} + i\gamma_4\frac{\partial^3\zeta}{\partial\xi\partial\eta^2} = \Lambda_1|\zeta|^2\zeta + i\Lambda_2|\zeta|^2\frac{\partial\zeta}{\partial\xi} + i\Lambda_3\zeta^2\frac{\partial\zeta^*}{\partial\xi} \\ &+\Lambda_{41}\zeta\frac{\partial}{\partial\xi}F^{-1}[\frac{F\frac{\partial}{\partial\xi}(|\zeta|^2)}{\overline{k}\tanh(\epsilon\overline{k}d_1)}] + \Lambda_{42}\zeta\frac{\partial}{\partial\xi}F^{-1}[\frac{F\frac{\partial}{\partial\xi}(|\zeta|^2)}{\overline{k}\tanh(\epsilon\overline{k}d_2)}], \end{aligned} \tag{20}$$

where the coefficients are given in the Appendix and F^{-1} means the inverse Fourier transform.

It is important to mention the small parameter ϵ, which describes both the slow modulations and the wave amplitude (see Grimshaw and Pullin (1985)). Here, $\epsilon\zeta_1$ is the complex wave amplitude, and to leading first order, the wave is described by $\epsilon\zeta_1 \exp i(kx - \omega t)$. So the first term on the right side of Eq. (20) is the order of magnitude $O(\epsilon^3)$, whereas the remaining terms are of order of magnitude $O(\epsilon^4)$, as the derivative increases the order by one $\left(\frac{\partial}{\partial x} = \epsilon\frac{\partial}{\partial x_1} = \epsilon\frac{\partial}{\partial\xi}\right)$.

The nonlinear spatio-temporal evolution of slowly modulated interfacial waves can be described by the nonlinear evolution equation provided that the wave steepness is small (<< 1) and the spectral bandwidth is narrow (<< 1). The derivation of Eq. (20) needs that ϵ is a small parameter and describes a balance between nonlinearity and wave dispersion about the dominant wavenumber k. Typically, one assumes that the wave steepness and the bandwidth are of the same order of magnitude $O(\epsilon)$, for which nonlinear and dispersive effects balance at the fourth-order $O(\epsilon^4)$.

Among the fourth-order dispersive and nonlinear terms in Eq. (20), only the last two terms on right side of that equation whose coefficients are Λ_{41} and Λ_{42} contribute to the stability results given by Eqs. (33) to (36). Accordingly, as far as stability properties are concerned, it is enough to consider the following simplified equation (see Dysthe (1979), page 113, Section 4).

$$\begin{aligned} &lli\frac{\partial\zeta}{\partial\tau} - \gamma_1\frac{\partial^2\zeta}{\partial\xi^2} + \gamma_2\frac{\partial^2\zeta}{\partial\eta^2} = \Lambda_1|\zeta|^2\zeta + \Lambda_{41}\zeta\frac{\partial}{\partial\xi}F^{-1}[\frac{F\frac{\partial}{\partial\xi}(|\zeta|^2)}{\overline{k}\tanh(\epsilon\overline{k}d_1)}] \\ &+ \Lambda_{42}\zeta\frac{\partial}{\partial\xi}F^{-1}[\frac{F\frac{\partial}{\partial\xi}(|\zeta|^2)}{\overline{k}\tanh(\epsilon\overline{k}d_2)}] \end{aligned} \tag{21}$$

To present the results plausible, it is useful to compare with other results. We can check that the coefficients γ_1, γ_2 and Λ_1 for $v = 0$ reduce to those of Grimshaw and Pullin (1985). Furthermore, for $r = 0$, $v = 0$ and infinite depth of fluid, the Eq. (20) reduces to an equation equivalent to Eq. (2) of Janssen (1983).

According to Brinch-Nielsen and Jonsson (1986), the finite depth assumption of $\tanh(\epsilon\overline{k}d_i)$ is $\epsilon\overline{k}d_i (i = 1, 2)$ and they have pointed out that the fourth-order terms of Eq. (20) do not contribute to the expression for imaginary part of Ω, where Ω is the perturbed frequency. Furthermore, for deep fluids, the conventional approximation is taken as $\tanh(\epsilon\overline{k}d_i) \approx 1 (i = 1, 2)$ and hence for deep fluids (Janssen 1983), we have

$$\frac{\partial}{\partial \xi}F^{-1}[\frac{F\frac{\partial}{\partial \xi}(|\zeta|^2)}{\bar{k}}] = H\frac{\partial}{\partial \xi}(|\zeta|^2), \tag{22}$$

where H is the two-dimensional Hilbert transform operator given by

$$Hg(\xi,\eta) = \frac{1}{2\pi}\iint_{-\infty}^{\infty}\frac{(\xi' - \xi)g(\xi',\eta')d\xi' d\eta'}{[(\xi' - \xi)^2 + (\eta' - \eta)^2]^{\frac{3}{2}}} \tag{23}$$

4 Stability analysis and results

(a) Third-order finite depths case:

The solution of uniform wave train of Eq. (20) is

$$\zeta = \frac{\alpha_0}{2}\exp\left(\frac{-i\alpha_0^2\Lambda_1\tau}{4}\right), \tag{24}$$

where α_0 is a real constant.

Its stability can be investigated by considering small perturbations ζ', θ' in amplitude and phase respectively

$$\zeta = \frac{\alpha_0}{2}(1+\zeta')\exp i(\theta' - \frac{\alpha_0^2\Lambda_1\tau}{4}) \tag{25}$$

We now suppose that $(\zeta', \theta') \propto \exp(-i\Omega\tau)$.

Substituting (25) in (20), linearizing with respect to ζ', θ' and then taking the Fourier transform of resulting equations defined by

$$(\bar{\zeta}', \bar{\theta}') = \iint_{-\infty}^{\infty}(\zeta', \theta')\exp[-i(\lambda\xi + \mu\eta)]\mathrm{d}\xi\mathrm{d}\eta, \tag{26}$$

we obtain finally the following nonlinear dispersion relation

$$\bar{P}_1 = [\bar{P}_2(\bar{P}_2 - \frac{\alpha_0^2\Lambda_1}{2})]^{\frac{1}{2}}, \tag{27}$$

where $\bar{P}_1 = \Omega - c_g\lambda, \bar{P}_2 = \gamma_1\lambda^2 - \gamma_2\mu^2$.

For instability we have

$$\bar{P}_2(\bar{P}_2 - \frac{\alpha_0^2\Lambda_1}{2}) < 0 \tag{28}$$

The growth rate of instability Ω_i, which is the imaginary part of perturbed frequency Ω, is given by

$$\Omega_i = \sqrt{\bar{P}_2(\frac{\alpha_0^2\Lambda_1}{2} - \bar{P}_2)} \tag{29}$$

For one-dimensional perturbation, we have $\mu = 0$, so that Ω_i reduces to

$$\Omega_i = \lambda\sqrt{\gamma_1(\frac{\alpha_0^2\Lambda_1}{2} - \gamma_1\lambda^2)} \tag{30}$$

and the expression for maximum growth rate of instability is given by

$$G_r = \frac{\Lambda_1\alpha_0^2}{4} \tag{31}$$

(b) Fourth-order deep fluids case:

In this case, we have the following nonlinear dispersion relation

$$\bar{Q}_1 = -\frac{\Lambda_2\alpha_0^2\lambda}{4} \pm [\bar{Q}_2\{\bar{Q}_2 - \frac{\alpha_0^2}{2}(\Lambda_1 - \frac{\Lambda_4\lambda^2}{\sqrt{\lambda^2+\mu^2}})\}]^{\frac{1}{2}} \tag{32}$$

in which $\bar{Q}_1 = \Omega - c_g\lambda + \gamma_3\lambda^3 + \gamma_4\lambda\mu^2, \bar{Q}_2 = \gamma_1\lambda^2 - \gamma_2\mu^2$ and $\Lambda_4 = \Lambda_{41} + \Lambda_{42}$.

The instability condition is given by

$$\bar{Q}_2[\bar{Q}_2 - \frac{\alpha_0^2}{2}(\Lambda_1 - \frac{\Lambda_4\lambda^2}{\sqrt{\lambda^2+\mu^2}})] < 0 \tag{33}$$

Now the growth rate of instability Ω_i is given by

$$\Omega_i = \sqrt{\bar{Q}_2[\frac{\alpha_0^2}{2}(\Lambda_1 - \frac{\Lambda_4\lambda^2}{\sqrt{\lambda^2+\mu^2}}) - \bar{Q}_2]} \tag{34}$$

The expressions for Ω_i and the maximum growth rate of instability G_r for one-dimensional perturbation ($\mu = 0$) respectively take the forms

$$\Omega_i = \lambda\sqrt{\gamma_1\{\frac{\alpha_0^2}{2}(\Lambda_1 - \Lambda_4|\lambda|) - \gamma_1\lambda^2\}} \tag{35}$$

$$G_r = \frac{\Lambda_1\alpha_0^2}{4}[1 - \frac{\Lambda_4\alpha_0}{2\sqrt{\gamma_1\Lambda_1}}] \tag{36}$$

In Figs. 1, 2, and 3, the maximum growth rate of instability G_r has been plotted against wave steepness α_0 for several values of depth uniform current v corresponding to both air–water interface and Boussinesq approximation. It is seen from Fig. 2 that G_r found from fourth-order equation increases with the enhancement of α_0 up to a certain value of α_0. Afterwards, the value of G_r reduces. Again, G_r found from third-order equation enhances steadily with the enhancement of α_0 (Dhar and Das 1994). G_r is observed to be notably much higher for velocity coming towards the critical value. Furthermore, in the case of air–water interface, G_r decreases as the depth d_1 of the upper fluid increases when the depth d_2 of the lower fluid is kept constant. Effects reverse to these are noticed in the case of a Boussinesq

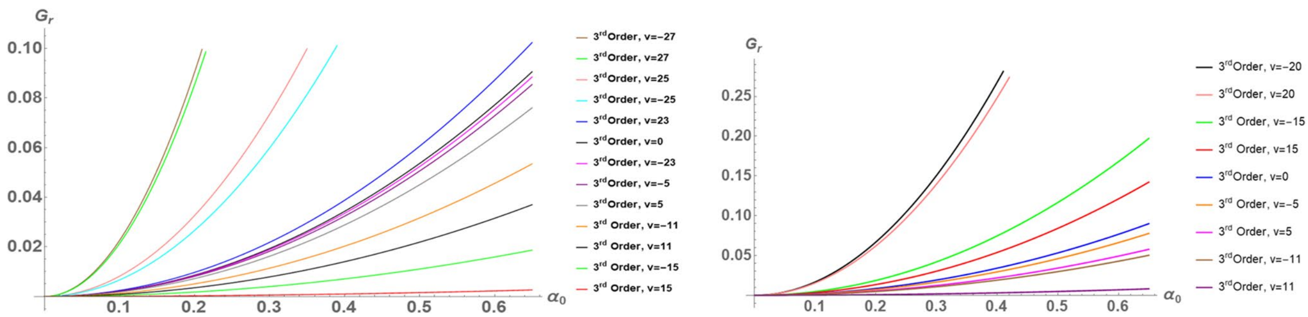

Fig. 1 Maximum growth rate of instability G_r as a function of α_0 for $r = 0.00129$; $d_1 = 2, d_2 = 2$, and $v = 0, \pm 5, \pm 11, \pm 15, \pm 23, \pm 25, \pm 27$ (left); $d_1 = 1, d_2 = 2$, and $v = 0, \pm 5, \pm 11, \pm 15, \pm 20$ (right)

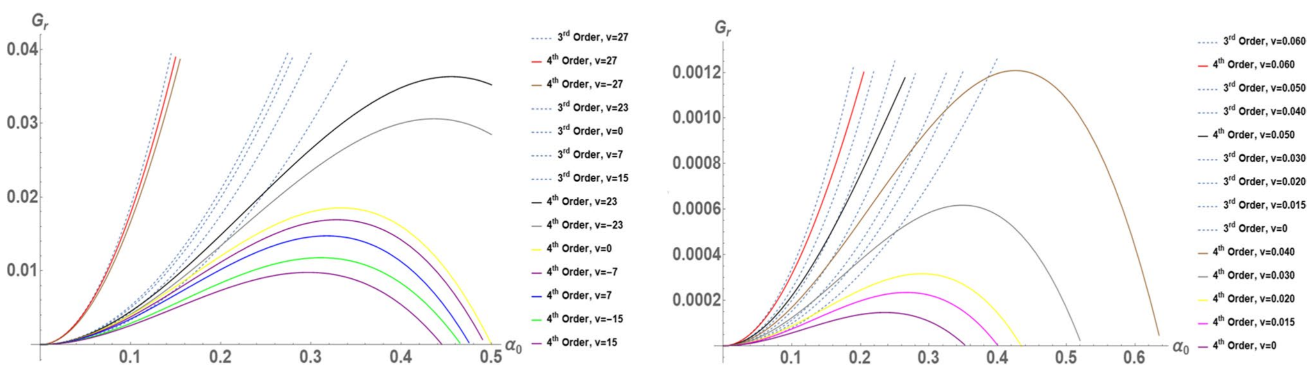

Fig. 2 Maximum growth rate of instability G_r as a function of α_0 for $d_1 \to \infty, d_2 \to \infty$ and $r = 0.00129$, $v = 0, \pm 7, \pm 15, \pm 23, \pm 27$ (left); $r \to 1$, $v = 0, 0.015, 0.020, 0.030, 0.040, 0.050, 0.060$ (right)

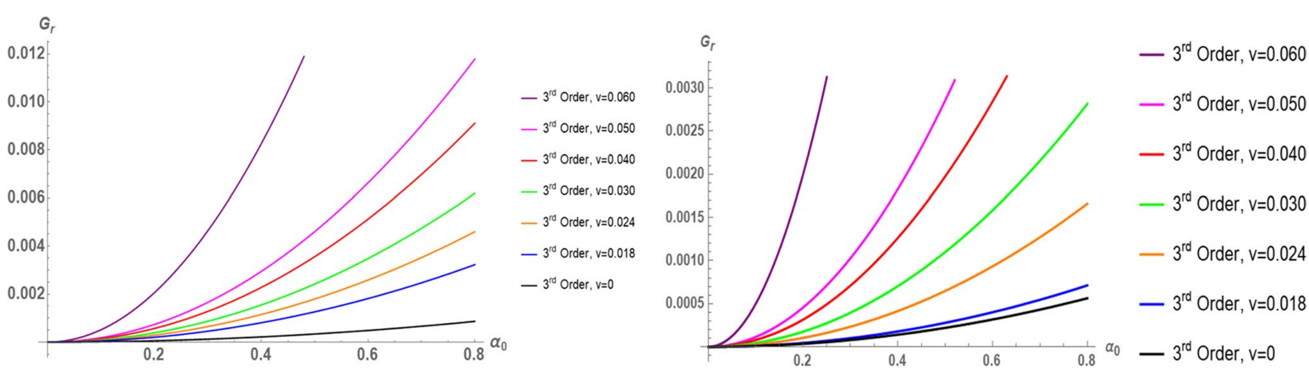

Fig. 3 Maximum growth rate of instability G_r as a function of α_0 for $r \to 1$; $d_1 = 4, d_2 = 2$, and $v = 0, 0.018, 0.024, 0.030, 0.040, 0.050, 0.060$ (left); $d_1 = 2, d_2 = 2$, and $v = 0, 0.018, 0.024, 0.030, 0.040, 0.050, 0.060$ (right)

approximation. As a check, for $r = 0$, the dimensionless growth rate Ω_i/α_0^2, we find from Eq. (30), is compared in Fig. 4 with that obtained by Liao et al. (2017) in Fig. 3. In that way, we can verify that this limiting case is reproduced exactly. From this figure, it is observed that the curve for $d_2 = 1.37$ indicates the disappearance of Benjamin-Feir instability as d_2 comes towards 1.363, which is compatible with notable classical theory.

Using the conditions (28) and (33), corresponding to third and fourth-order results respectively, we have drawn some instability regions for infinite depth of fluids in Figs. 5, 6, 7, 8, 9, 10, 11, and 12 for several values of depth uniform current v and wave steepness α_0. From these figures, it is observed that in both the cases of air–water interface and Boussinesq approximation, the instability region increases in size as α_0 increases whereas this region diminishes in size

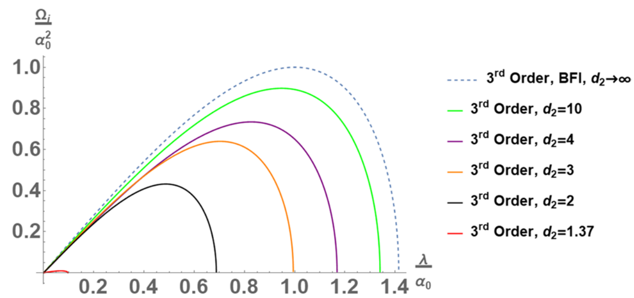

Fig. 4 Dimensionless growth rate $\frac{\Omega_i}{\alpha_0^2}$ as a function of $\frac{\lambda}{\alpha_0}$ for different values of water depth d_2 and $v = 0, r = 0, d_1 \to \infty$. BFI indicates the Benjamin-Feir instability in infinite depth of water

as v increases. Also, the fourth-order effect affords a shrinkage of the instability region and a decrease in the growth rate (see Fig. 2) giving a stabilizing effect. An important and interesting particular case is the water waves which is obtained for $r = 0$ and is shown in Fig. 9. In this figure the fourth-order equation gives much better results which are closer to the exact numerical results obtained by McLean et al. (1981) in Fig. 1a, b for $\alpha_0 = 0.2$ and 0.4 than that given by the third-order evolution equation. Furthermore, the instability regions presented in Fig. 10 for $r = 0.1$ and 0.9, corresponding to fourth-order result, are found to almost overlap with the regions found by Yuen (1984) (see Fig. 4a and d) (Yuen 1984) from exact numerical computations. We therefore conclude that fourth-order nonlinear evolution equation gives fairly excellent long wave length region of type I instability of interfacial gravity waves for small but finite wave steepness.

Again, in Figs. 11 and 12, we have drawn some instability regions for water waves for two finite values of depth $d_2 = 2, 1.4$, one greater than 1.363 and other near to 1.363, following McLean (1982a). In Fig. 11, three instability regions drawn by us have the same value of the parameters as those of Figs. 2a, b, and c of McLean (1982a) and these regions are observed to nearly overlap with each other. These regions correspond to the long wavelength regions of type I instability obtained by McLean (1982a) from numerical computation. It is significant to note that Fig. 12 indicates the disappearance of Benjamin-Feir instability region as $d_2 = 1.363$ is approached for long wavelength, two-dimensional perturbations and small wave steepness, as predicted by Whitham (1967).

In Figs. 13, 14, 15, and 16, we have portrayed the contour plots of growth rate of instability, $G_r = Im(\Omega)$ in the (λ, μ) plane for different values of wave steepness α_0 and velocity v. From these contour plots, we have observed that for both the cases of air–water interface and Boussinesq approximation, the growth rate G_r increases with the velocity v, when the wave steepness α_0 is kept constant and further the growth rate G_r increases with the wave steepness α_0, when the velocity v is kept constant. We have found similar characteristics for both finite and infinite depth of fluids. Finally, in all Figs. 13, 14, 15, and 16, it is seen that the region of instability is symmetric about the lines $\lambda = 0$ and $\mu = 0$.

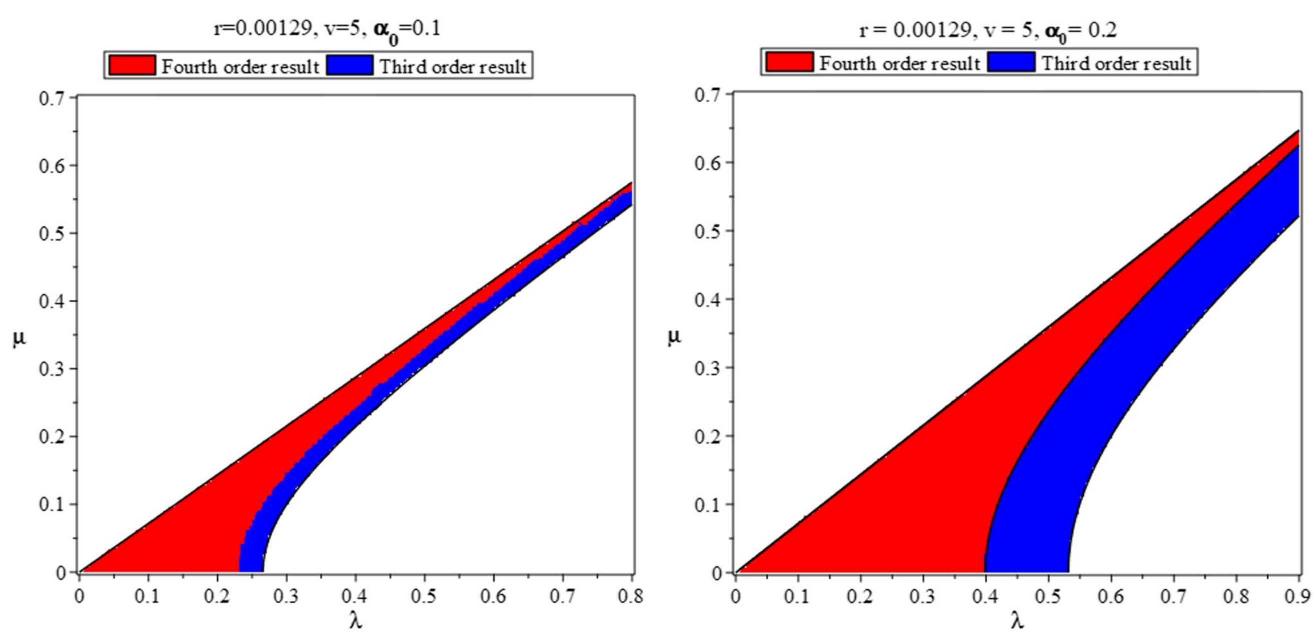

Fig. 5 Instability regions in the (λ, μ) plane for $r = 0.00129, d_1 \to \infty, d_2 \to \infty, v = 5, \alpha_0 = 0.1$ (left), $\alpha_0 = 0.2$ (right)

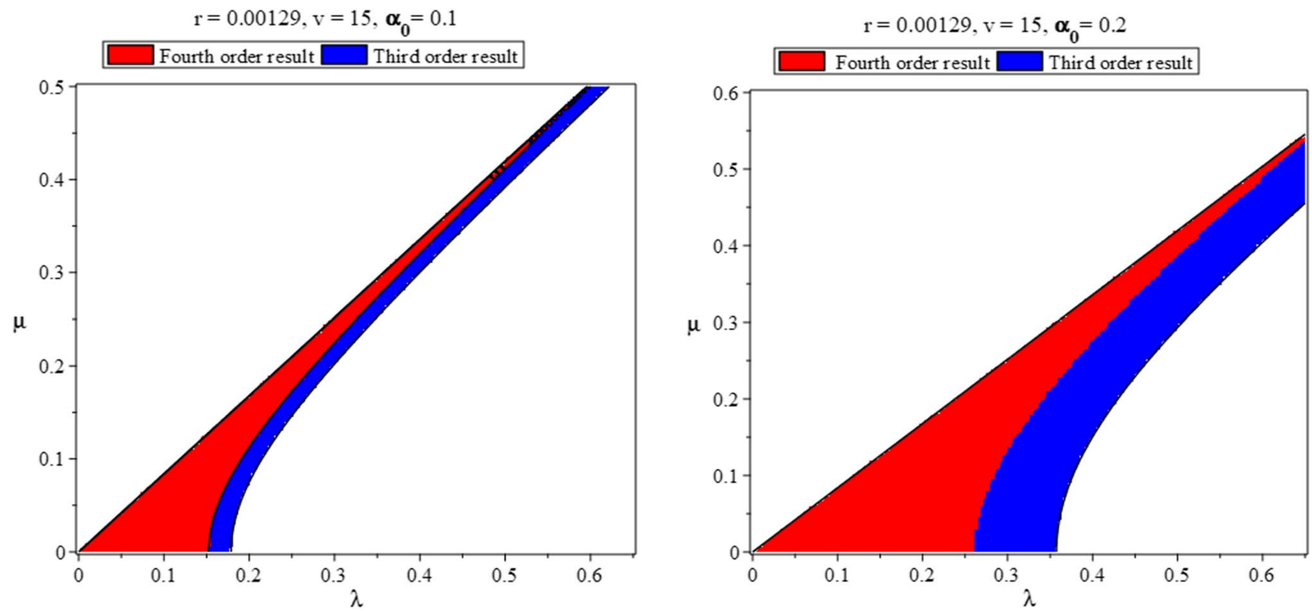

Fig. 6 Instability regions in the (λ, μ) plane for $r = 0.00129$, $d_1 \to \infty, d_2 \to \infty$, $v = 15$, $\alpha_0 = 0.1$ (left), $\alpha_0 = 0.2$ (right)

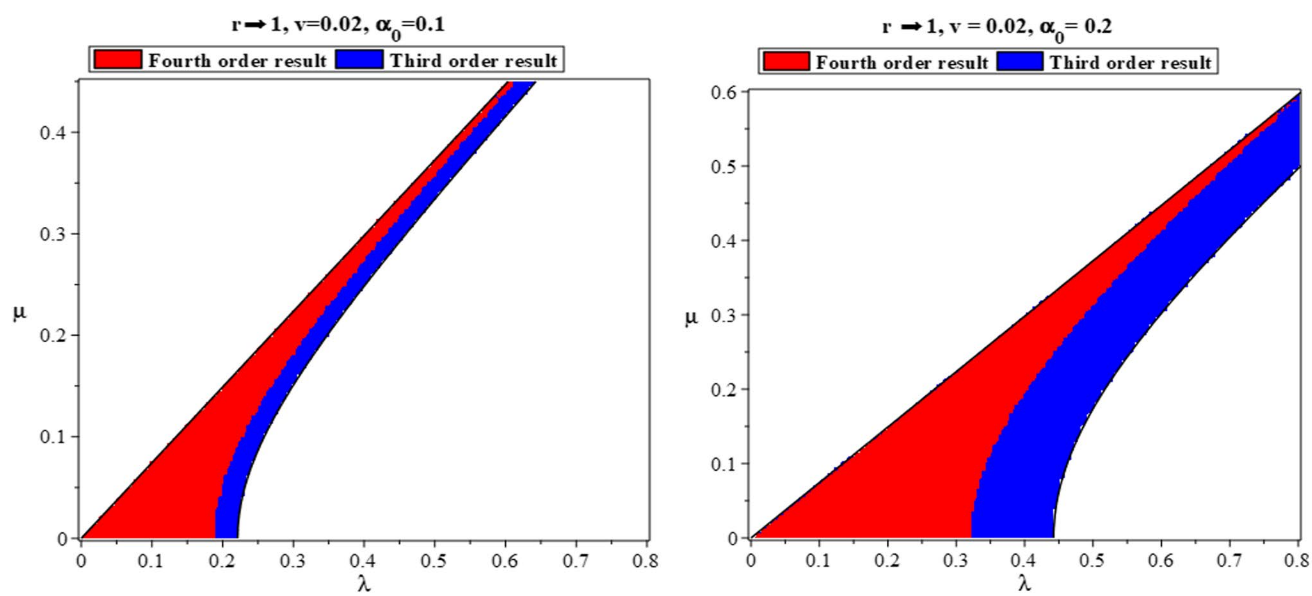

Fig. 7 Instability regions in the (λ, μ) plane for $r \to 1$, $d_1 \to \infty, d_2 \to \infty$, $v = 0.02$, $\alpha_0 = 0.1$ (left), $\alpha_0 = 0.2$ (right)

5 Impact of depth uniform current on Peregrine breather

It is well known that the instability due to modulation of gravity waves can be modelled by the nonlinear Schrödinger equation, and the easiest analytical solution of this equation is the Peregrine breather. In third order, the nonlinear Schrödinger Eq. (20) can be written as

$$i\frac{\partial \zeta}{\partial \tau} - \gamma_1 \frac{\partial^2 \zeta}{\partial \xi^2} + \gamma_2 \frac{\partial^2 \zeta}{\partial \eta^2} = \Lambda_1 |\zeta|^2 \zeta \tag{37}$$

The dimensionless form of Eq. (37) in one spatial dimension can be expressed as

$$i\zeta'_{\tau'} + \zeta'_{\xi'\xi'} + 2|\zeta'|^2 \zeta' = 0, \tag{38}$$

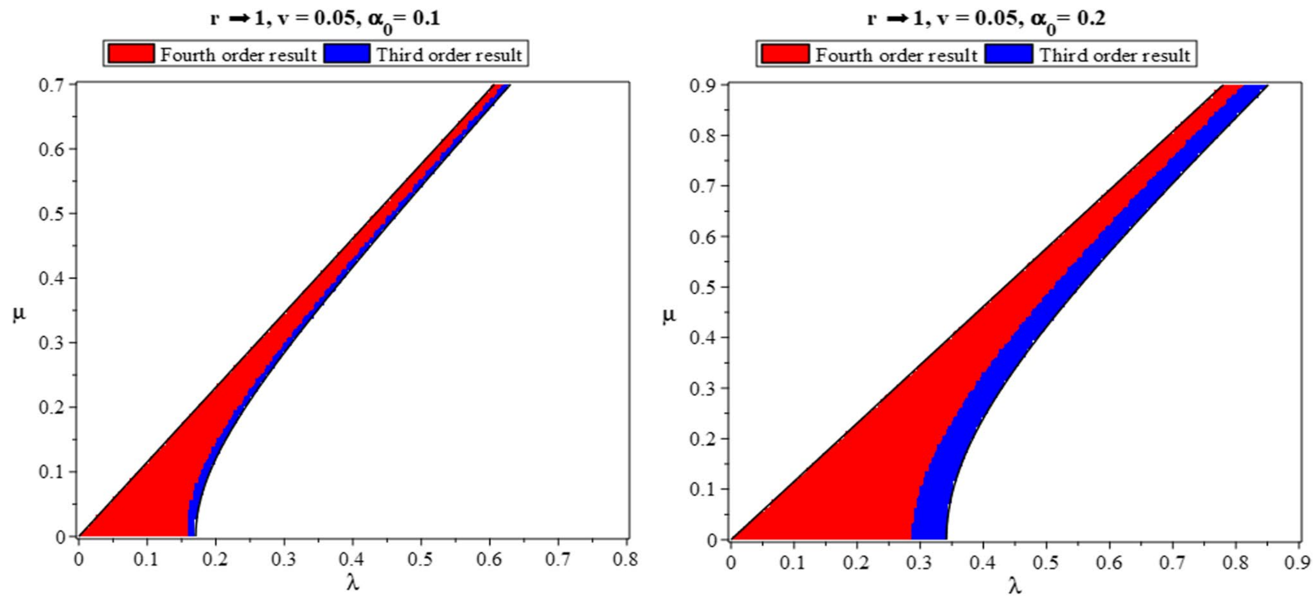

Fig. 8 Instability regions in the (λ, μ) plane for $r \to 1$, $d_1 \to \infty$, $d_2 \to \infty$, and $v = 0.05$; $\alpha_0 = 0.1$ (left), $\alpha_0 = 0.2$ (right)

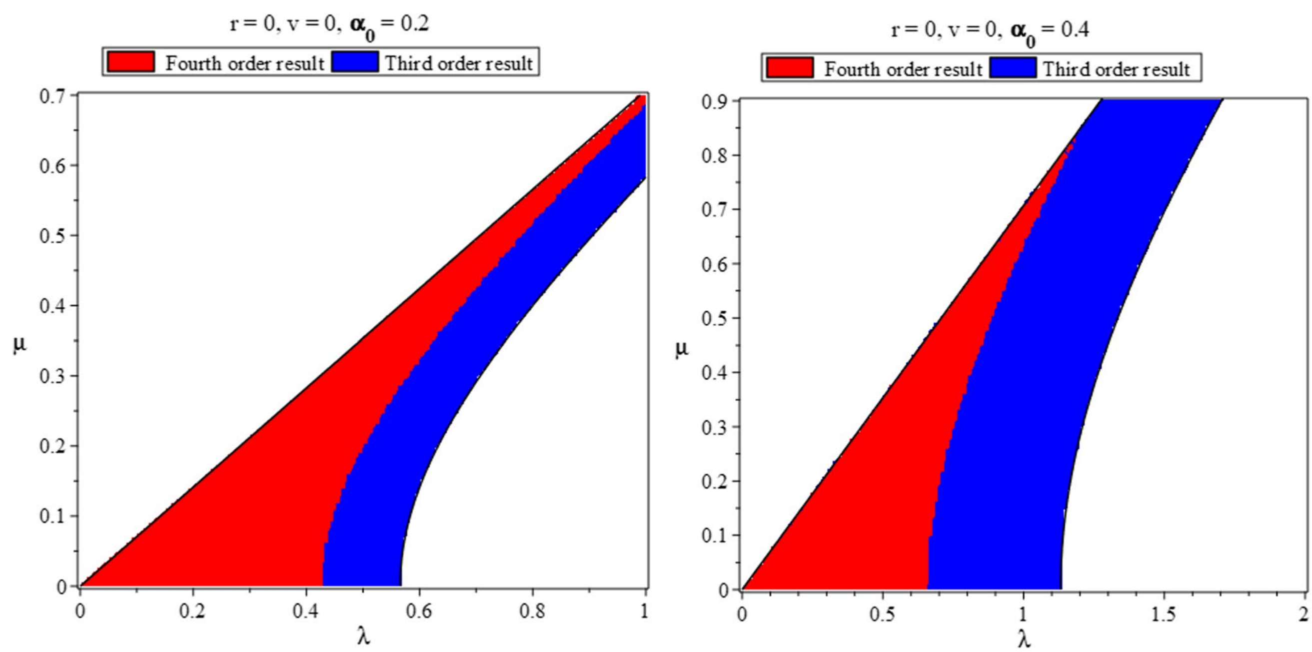

Fig. 9 Instability regions in the (λ, μ) plane for $r = 0$, $d_2 \to \infty$, and $v = 0$; $\alpha_0 = 0.2$ (left), $\alpha_0 = 0.4$ (right)

which is obtained by employing the transformation on the variables as follows

$$\xi' = \frac{1}{2}\alpha_0\sqrt{\frac{2\Lambda_1}{\gamma_1}}\xi, \tau' = -\frac{1}{2}\Lambda_1\alpha_0^2\tau, \zeta' = \frac{\zeta}{\alpha_0} \tag{39}$$

Here ξ' denotes the normalized coordinate and the normalized time is denoted as τ'. The Peregrine breather solution (Peregrine 1983 (Peregrine 1983)) of Eq. (38) is

$$\zeta'(\xi', \tau') = \{\frac{4(1 + 4i\tau')}{1 + 4\xi'^2 + 16\tau'^2} - 1\}\exp(2i\tau') \tag{40}$$

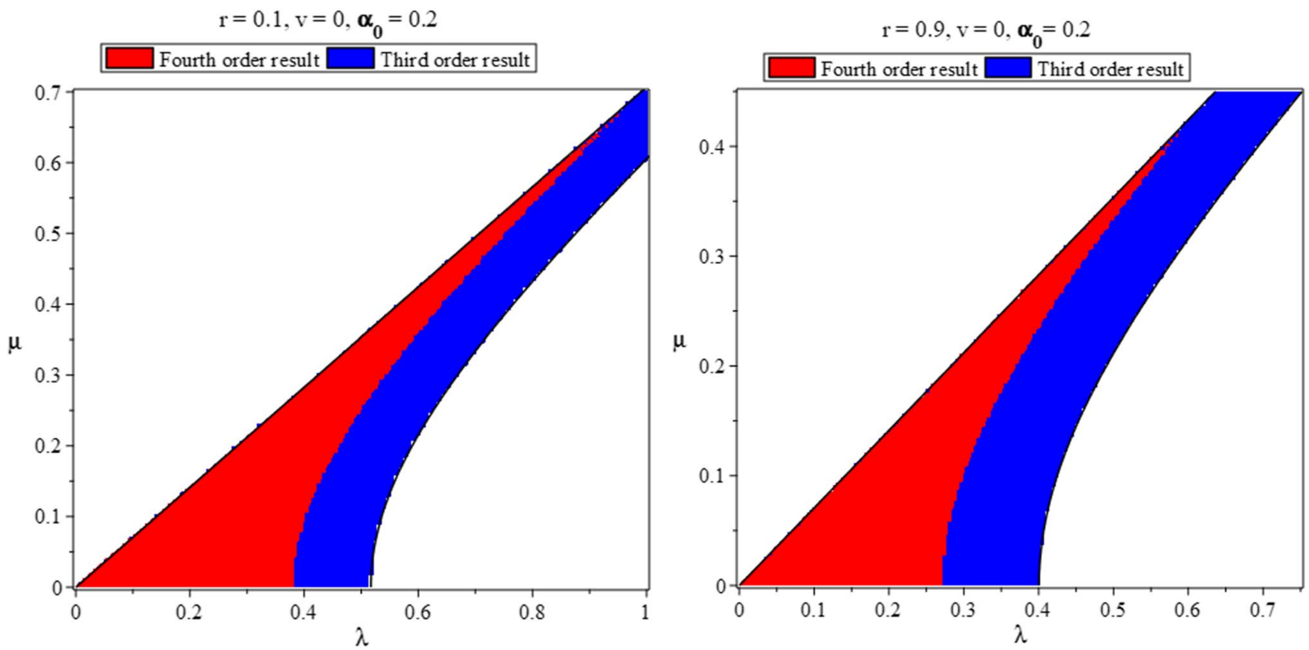

Fig. 10 Instability regions in the (λ, μ) plane for $\alpha_0 = 0.2$ and $v = 0, d_1 \to \infty, d_2 \to \infty$; $r = 0.1$ (left), $r = 0.9$ (right)

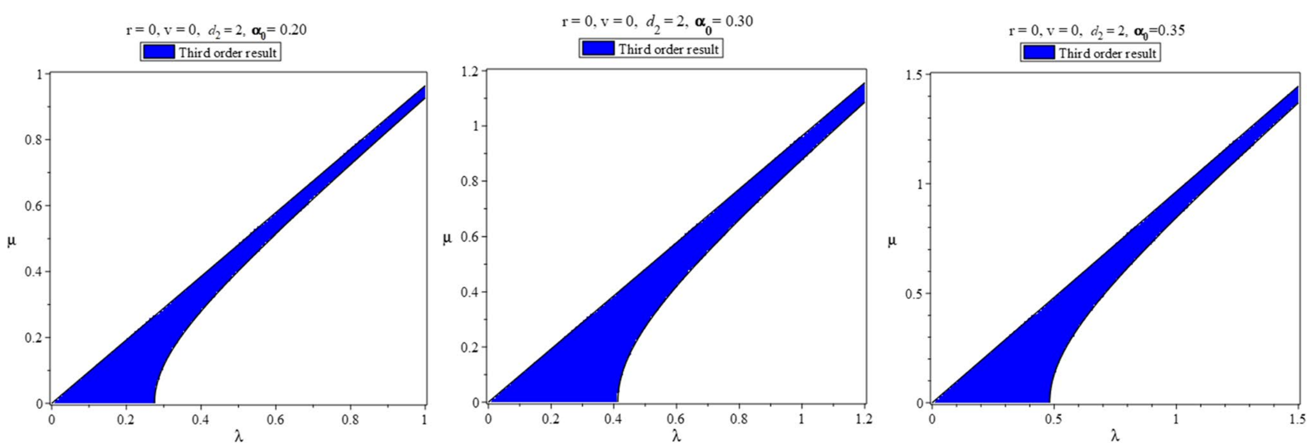

Fig. 11 Instability regions in the (λ, μ) plane for $r = 0$, $v = 0$, $d_2 = 2$, and $\alpha_0 = 0.20, 0.30, 0.35$

which is localized both in space and time. Using the transformations given by (39), we find the dimensional form of Peregrine breather solution as

$$\zeta(x_1, t_1) = \alpha_0 \exp(-i\Lambda_1 \alpha_0^2 t_1) \times \{ \frac{4\gamma_1(1-2i\Lambda_1\alpha_0^2 t_1)}{\gamma_1+2\Lambda_1\alpha_0^2(x_1-c_g t_1)^2+4\gamma_1\Lambda_1^2\alpha_0^4 t_1^2} - 1 \} \tag{41}$$

The significant point of the Peregrine breather is that its maximum value is achieved at a single point in both the spatial and time domains and declines exponentially outside the localized region.

In Figs. 17, 18, 19, 20, 21, 22, and 23, we have plotted the breather solution for different values of depth uniform current and fluid depths in space and time domains. In both the cases of air–water interface as well as Boussinesq approximation, the breather span increases as the depth d_1 of the upper fluid decreases as seen from Figs. 17 and 18. Furthermore, from the corresponding sub-figures of Figs. 17 and 18, it is found that the breather span increases with the increment of absolute value of the velocity v in the case of air–water interface, whereas opposite characteristic has been observed for Boussinesq approximation. In Fig. 17 (left), the dashed line shows the envelope of the Peregrine breather solution for $r = 0, d_2 = 2, v = 0.2$, which is reproduced exactly as that of Liao et al. (2017) in Fig. 10(a).

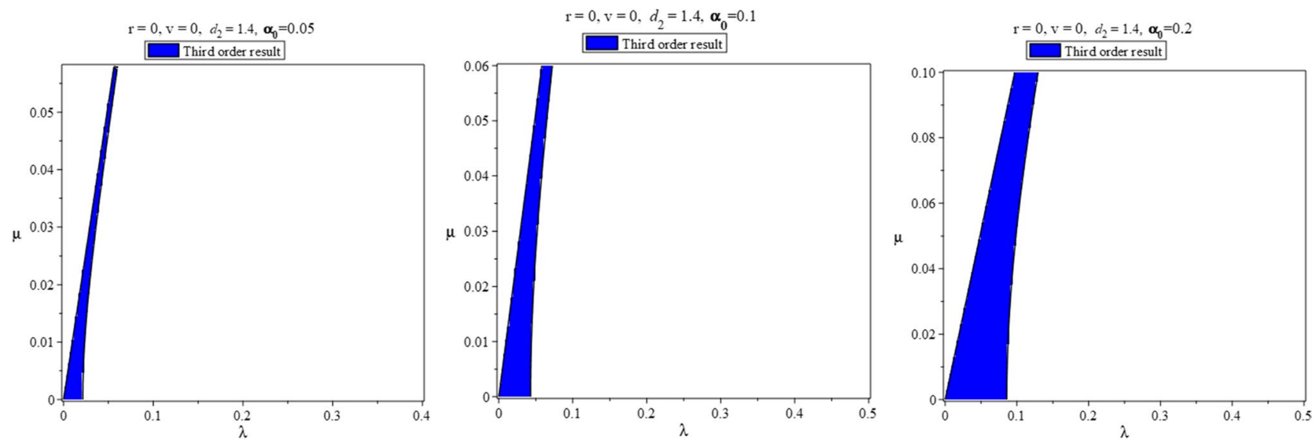

Fig. 12 Instability regions in the (λ, μ) plane for $r = 0$, $v = 0$, $d_2 = 1.4$, and $\alpha_0 = 0.05, 0.1, 0.2$

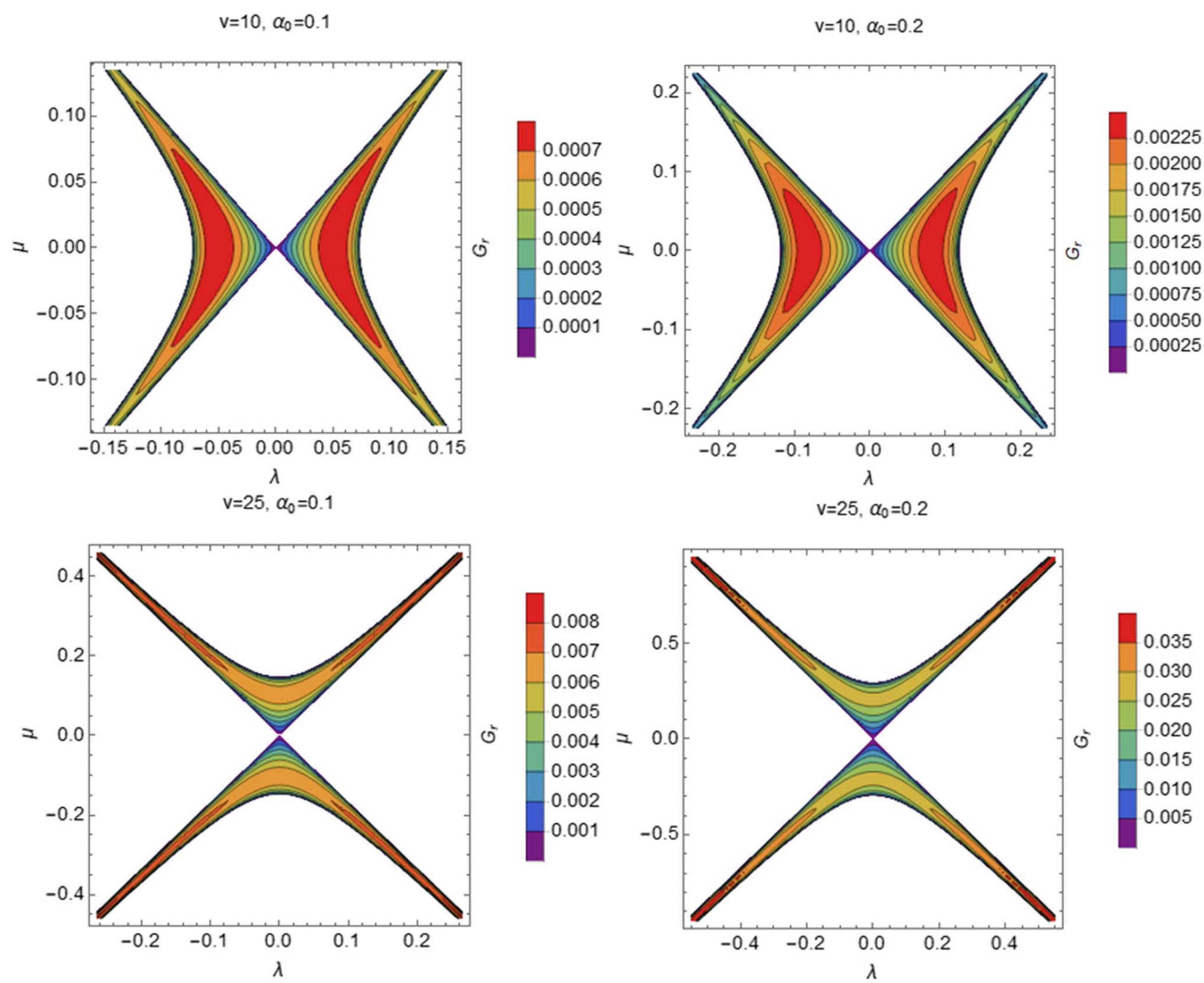

Fig. 13 Contour plot of instability growth rate $G_r = Im(\Omega)$ in the (λ, μ) plane for $r = 0.00129$, $d_1 = 2, d_2 = 2$, $\alpha_0 = 0.1, 0.2$, and $v = 10, 25$

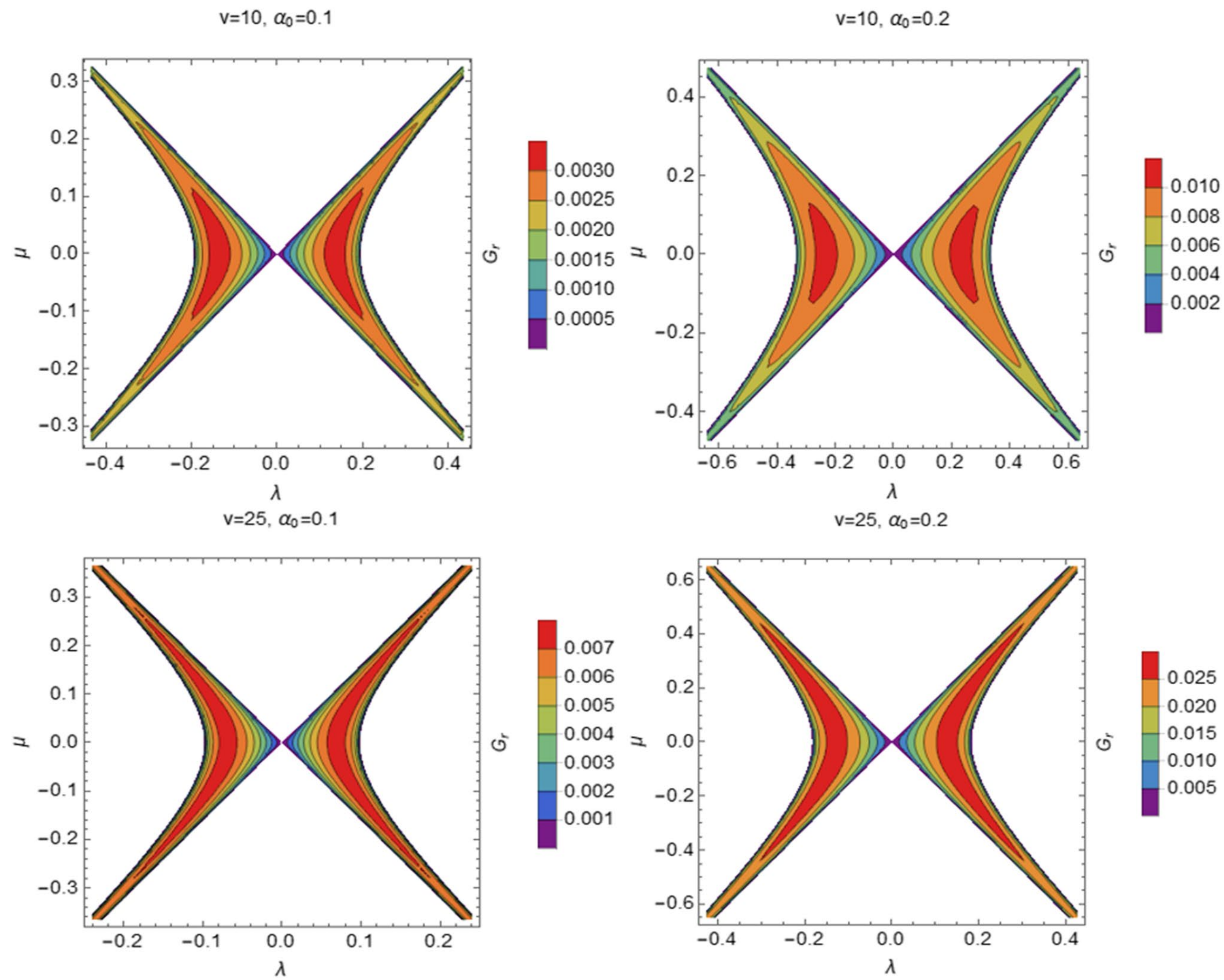

Fig. 14 Contour plot of instability growth rate $G_r = Im(\Omega)$ in the (λ, μ) plane for $r = 0.00129$, $d_1 \to \infty$, $d_2 \to \infty$, $\alpha_0 = 0.1, 0.2$, and $v = 10, 25$

Again, for infinite depth of fluids, we have observed from Fig. 19 (left) that the breather span increases as the absolute value of the velocity increases. An opposite effect is observed for Boussinesq approximation as seen from Fig. 19 (right). These aforesaid characteristics have also been confirmed from the Figs. 20, 21, and 22. Finally, Fig. 23 shows the Peregrine breather solution for $r = 0, d_2 = 2$, $v = 0.2$, which is reproduced here as obtained by Liao et al. (2017) in Fig. 9(d).

6 Conclusion

In the present paper, we have derived a $(2+1)$-dimensional fourth-order nonlinear evolution equation for interfacial gravity waves of a two-layer fluid domain with the lower fluid having a depth uniform current v. We have discussed the stability analysis of the plane progressive wave for both the cases of air–water interface ($r = 0.00129$) and Boussinesq approximation ($r \to 1$) and also for finite and infinite depths of fluids. The present fourth-order evolution equation affords considerably better results consistent with the exact numerical results obtained by McLean et al. (1981) and Yuen (1984) than that given by the third-order evolution equation. Furthermore, the fourth-order effect produces a contraction of instability region and a decrease in the growth rate giving a stabilizing effect. Therefore, it is important to note that the long wavelength instability region of interfacial gravity waves for small but finite wave steepness has been analyzed by Yuen (1984), which can be obtained analytically from the fourth-order nonlinear evolution equation. The contour figures have been plotted here to describe the effects of wave steepness α_0 and the velocity v of the lower fluid on the growth rate of instability. Additionally, starting from third-order $(1+1)$-dimensional NLSE, we have determined the effect of depth uniform current on Peregrine breather. In the end, it is important to note that in

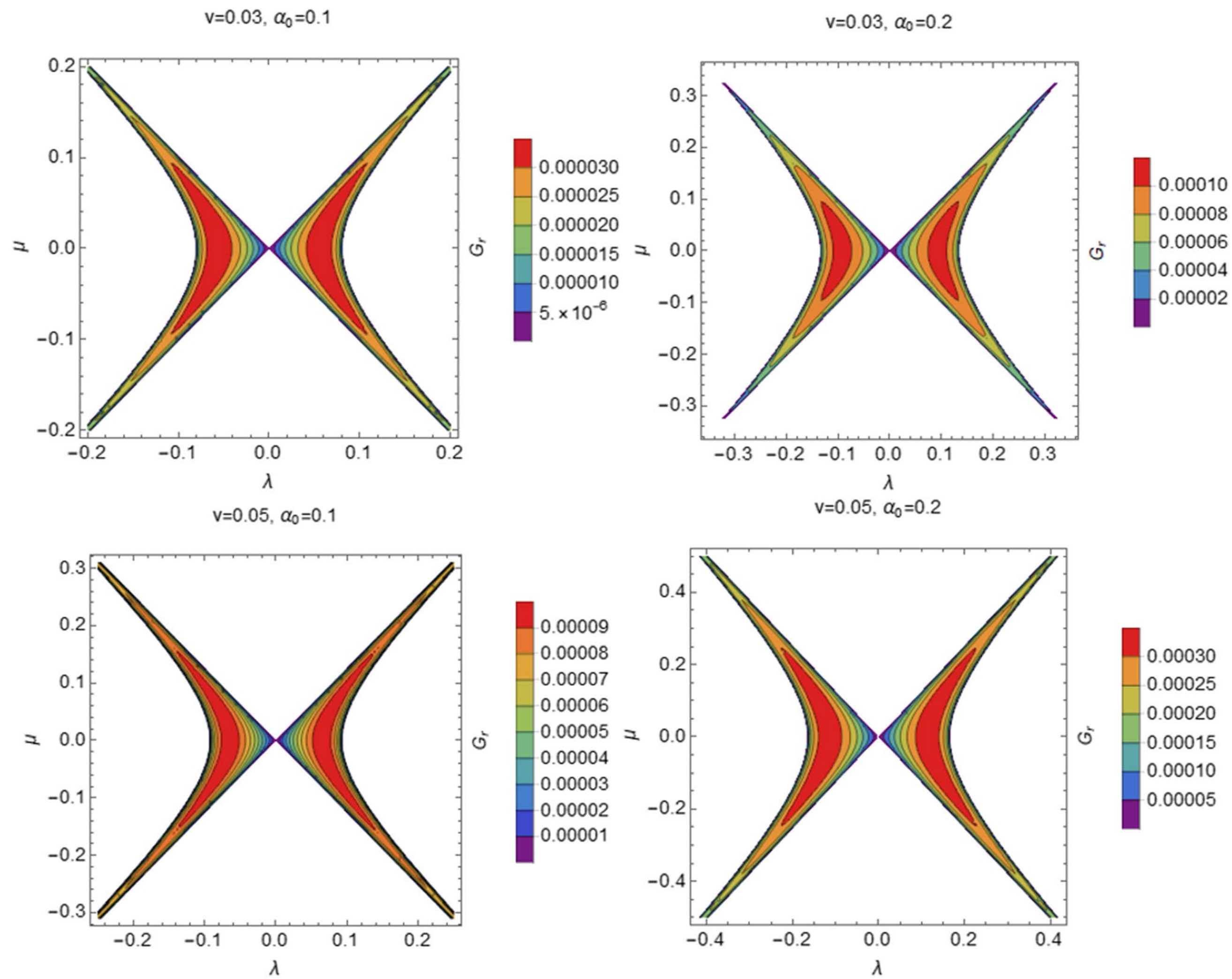

Fig. 15 Contour plot of instability growth rate $G_r = Im(\Omega)$ in the (λ, μ) plane for $r \to 1$, $d_1 = 2$, $d_2 = 2$, $\alpha_0 = 0.1, 0.2$, and $v = 0.03, 0.05$

the case of air–water interface, the dimension of the breather is spreaded significantly on following currents.

Appendix

The coefficients appearing in Eq. (20)

$$\gamma_1 = -\frac{1}{2}\left(\frac{\mathrm{d}c_g}{\mathrm{d}k}\right)_{l=0k=1} = \frac{1}{f_\omega}[(\sigma_1 + r\sigma_2)c_g^2 + 2\omega c_g\{d_1(1-\sigma_1^2) + rd_2(1-\sigma_2^2)\} - 2\delta_3 v c_g$$
$$-\omega^2\{\sigma_1 d_1^2(1-\sigma_1^2) + r\sigma_2 d_2^2(1-\sigma_2^2)\} - (1-r)(\delta_1+\delta_4-\delta_5)$$
$$-2\omega d_1(1-\sigma_1^2)(1-\sigma_1 d_1)v + \{\delta_3 + d_1(1-\sigma_1^2)(1-\sigma_1 d_1)\}v^2],$$

$$\gamma_2 = \frac{(1-r)\sigma_1\sigma_2}{2f_\omega}, \gamma_3 = -\frac{1}{6}\left(\frac{\mathrm{d}^2 c_g}{\mathrm{d}k^2}\right)_{\substack{l=0\\k=1}},$$

$$\gamma_4 = \frac{1}{2f_\omega}\left[(f_{\omega ll}c_g + f_{kll}) - \frac{(f_{\omega\omega}c_g + f_{\omega k})f_{ll}}{f_\omega}\right]_{\substack{l=0\\k=1}},$$

$$\Lambda_1 = \frac{1}{2\sigma_1^3\sigma_2^3 f_\omega}[2\{(\omega-v)^2\sigma_1^2(1-\sigma_2^2) - r\omega^2(1-\sigma_1^2)\sigma_2^2 + \frac{2\sigma_1^2\sigma_2}{d_2}(\omega-v)(c_g-v)$$
$$-\frac{2r\sigma_1\sigma_2^2\omega c_g}{d_1}\}^2/\{\frac{(c_g-v)^2}{d_2} + \frac{rc_g^2}{d_1} - (1-r)\} - 8\sigma_1^2\sigma_2^2\{\frac{(\omega-v)^2\sigma_1^2}{d_2} + \frac{r\omega^2\sigma_2^2}{d_1}\}$$
$$+\frac{\{(\omega-v)^2\sigma_1^2(3-\sigma_2^2) - r\omega^2(3-\sigma_1^2)\sigma_2^2\}^2}{\{(\omega-v)^2\sigma_2 + r\omega^2\sigma_1\}} - 4\sigma_1\sigma_2\{(\omega-v)^2\sigma_1^3(1-2\sigma_2^2)$$
$$+r\omega^2(1-2\sigma_1^2)\sigma_2^3\}],$$

$$\Lambda_{41} = \frac{4r\sigma_2^2\omega^2}{f_\omega}, \Lambda_{42} = \frac{4\sigma_1^2(\omega-v)^2}{f_\omega}, \Lambda_4 = \Lambda_{41} + \Lambda_{42},$$

where $\delta_1 = \sigma_1 d_2(1-\sigma_2^2) + \sigma_2 d_1(1-\sigma_1^2), \delta_3 = \sigma_1 + d_1(1-\sigma_1^2), \delta_4 = d_1 d_2(1-\sigma_1^2)(1-\sigma_2^2), \delta_5 = [d_1^2(1-\sigma_1^2) + d_2^2(1-\sigma_2^2)]\sigma_1\sigma_2.$

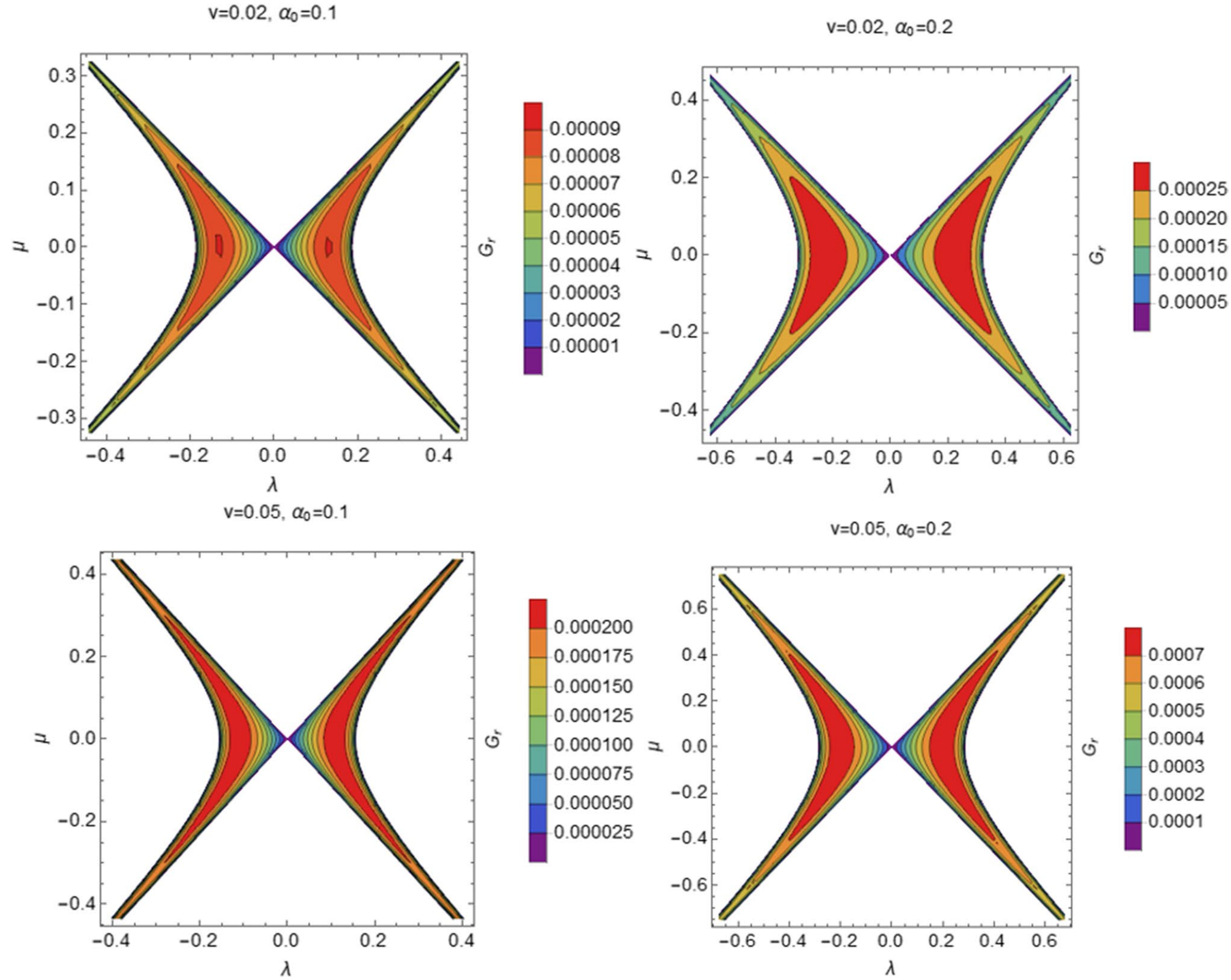

Fig. 16 Contour plot of instability growth rate $G_r = Im(\Omega)$ in the (λ, μ) plane for $r \to 1$, $d_1 \to \infty, d_2 \to \infty$, $\alpha_0 = 0.1, 0.2$, and $v = 0.02, 0.05$

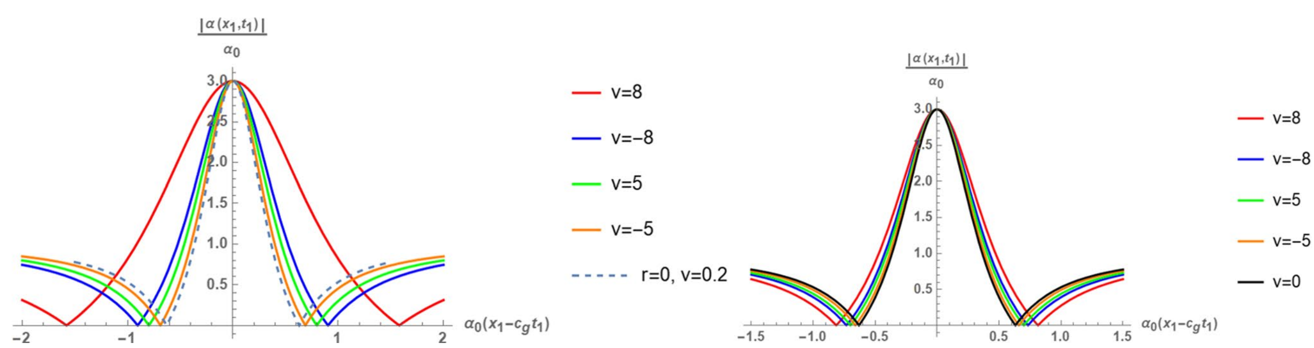

Fig. 17 $|\alpha(x_1, t_1)|/\alpha_0$ vs $\alpha_0(x_1 - c_g t_1)$ plot for $r = 0.00129$, $d_2 = 2$ and $d_1 = 1$ (left), $d_1 = 2$ (right)

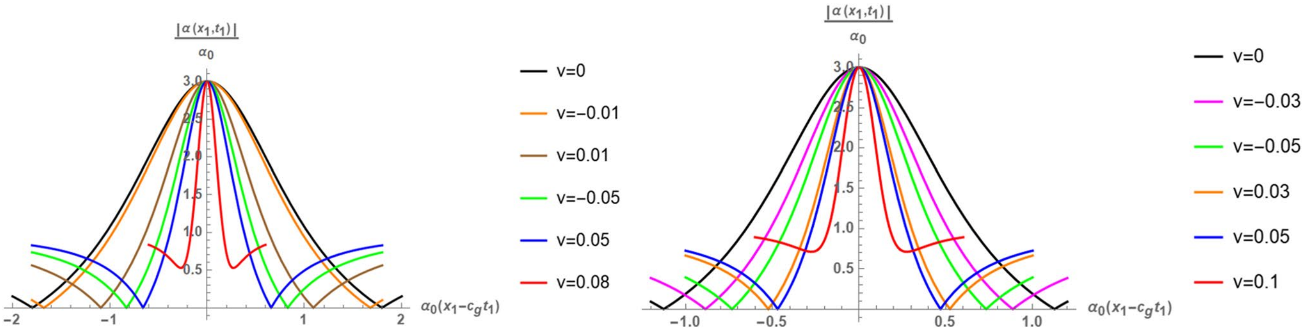

Fig. 18 $|\alpha(x_1, t_1)|/\alpha_0$ vs $\alpha_0(x_1 - c_g t_1)$ plot for $r \to 1$, $d_2 = 2$ and $d_1 = 3$ (left), $d_1 = 5$ (right)

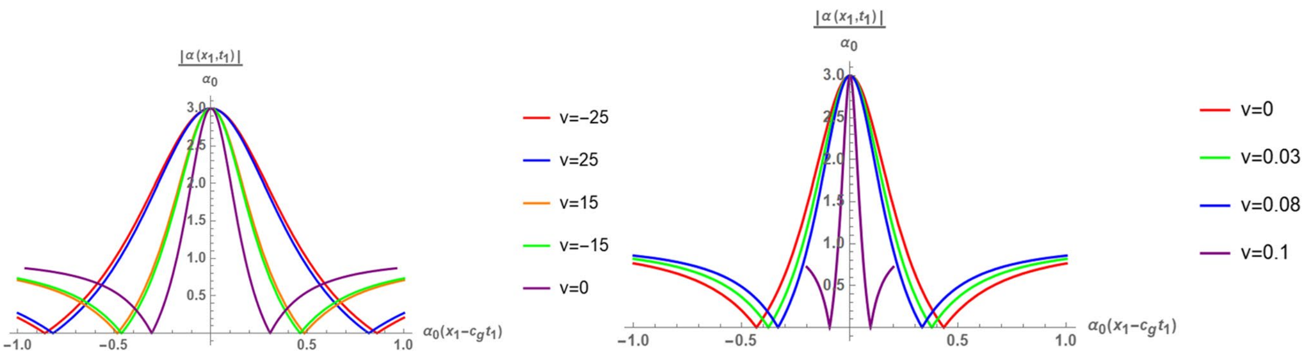

Fig. 19 $|\alpha(x_1, t_1)|/\alpha_0$ vs $\alpha_0(x_1 - c_g t_1)$ plot for $d_1 \to \infty$,$d_2 \to \infty$, $r = 0.00129$, $v = 0, \pm 15, \pm 25$ (left) and $r \to 1$, $v = 0, 0.03, 0.08, 0.1$ (right)

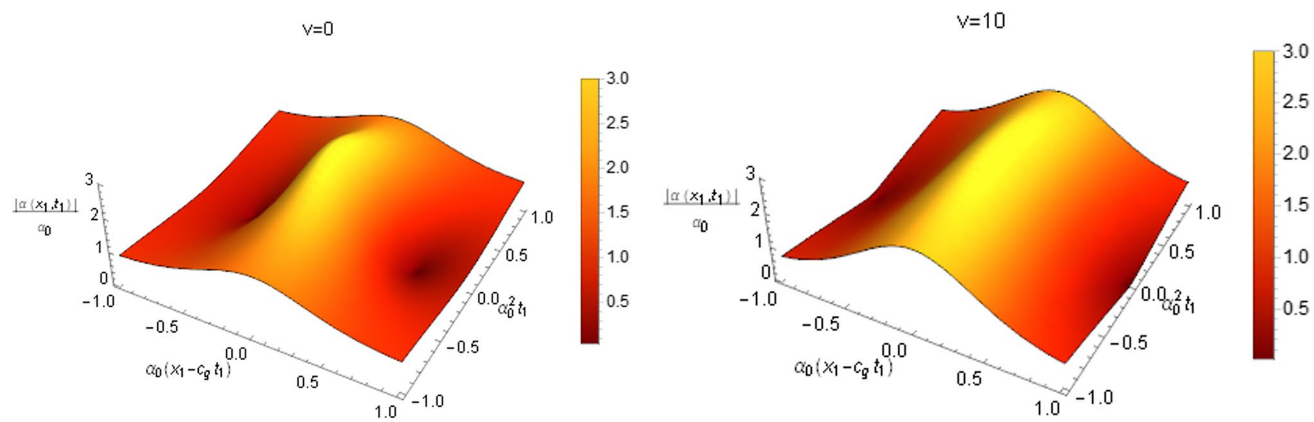

Fig. 20 Peregrine breather for $r = 0.00129$, $d_1 = 2, d_2 = 2$, $v = 0$ (left), $v = 10$ (right)

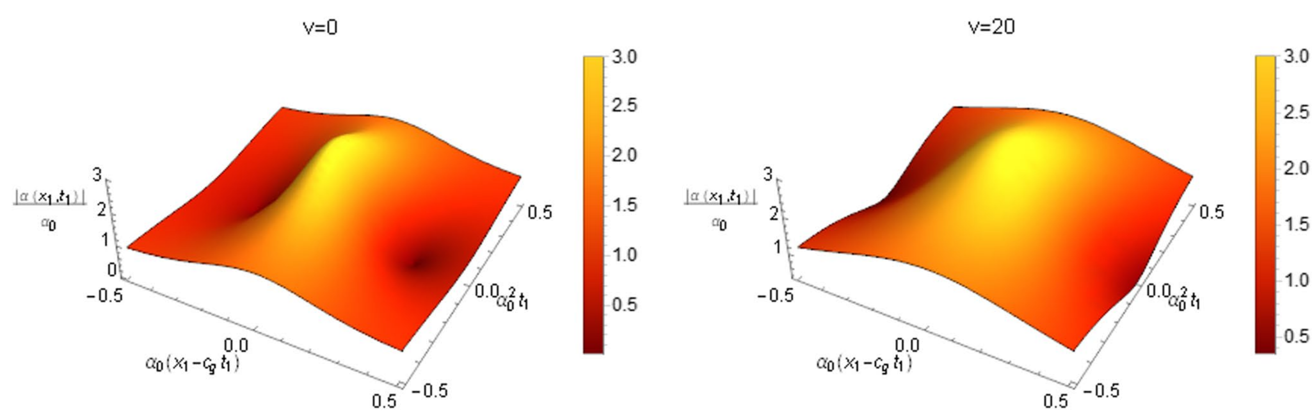

Fig. 21 Peregrine breather for $r = 0.00129$, $d_1 \to \infty, d_2 \to \infty$, $v = 0$ (left), $v = 20$ (right)

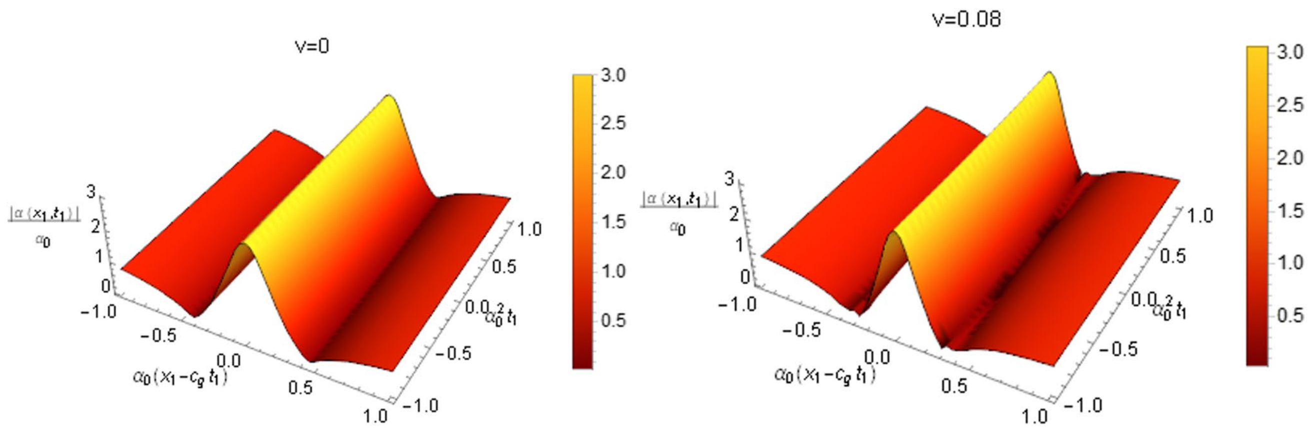

Fig. 22 Peregrine breather for $r \to 1$, $d_1 \to \infty$, $d_2 \to \infty$, $v = 0$ (left), $v = 0.08$ (right)

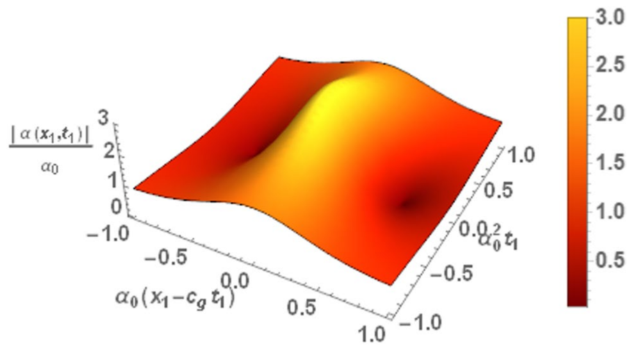

Fig. 23 Peregrine breather for $r = 0$, $d_2 = 2$, and $v = 0.2$

Acknowledgements The authors are grateful to the reviewers for their useful comments towards the improvement of the manuscript.

Data availability Data sharing is not applicable to this article as no datasets were generated or analyzed during the current study.

Declarations

Conflict of interest The authors declare no competing interests.

References

Bretherton FP, Garrett CJR (1968) Wavetrains in inhomogeneous moving media. Proc R Soc London Ser A 302:529–554

Brinch-Nielsen U, Jonsson IG (1986) Fourth order evolution equations and stability analysis for stokes waves on arbitrary water depth. Wave Motion 8:455–472

Dhar AK, Das KP (1990) A fourth-order evolution equation for deep water surface gravity waves in the presence of wind blowing over water. Phys Fluids A 2(5):778–783

Dhar AK, Das KP (1994) Stability analysis from fourth order evolution equation for small but finite amplitude interfacial waves in the presence of a basic current shear. J Aust Math Soc Ser B Appl Math 35:348–365

Dysthe KB (1979) Note on a modification to the nonlinear schrödingerr equation for application to deep water waves. Proc R Soc Lond A 369:105–114

Gerber M (1987) The benjamin-feir instability of a deep-water stokes wavepacket in the presence of a non-uniform medium. J Fluid Mech 176:311–332

Grimshaw RHJ, Pullin DI (1985) Stability of finite-amplitude interfacial waves, part 1. modulational instability for small-amplitude waves. J Fluid Mech 160:297–315

Hjelmervik K, Trulsen K (2009) Freak wave statistics on collinear currents. J Fluid Mech 637:267–284

Huang Z, Mei C (2003) Effects of surface waves on a turbulent current over a smooth or rough seabed. J Fluid Mech 497:253–287

Janssen P (1983) On a fourth-order envelope equation for deep-water waves. J Fluid Mech 126:1–11

Kantardgi I (1995) Effect of depth current profile on wave parameters. Coast Eng 26:195–206

Liao B, Dong G, Ma Y, Gao JL (2017) Linear-shear-current modified schrodinger equation for gravity waves in finite water depth. Phys Rev E 96:043111

Liu PLF, Dingemans MW, Kostense JK (1990) Long-wave generation due to the refraction of short-wave groups over a shear current. J Phys Oceanogr 20:53–59

Longuet MS, Stewart RW (1961) The changes in amplitude of short gravity waves on steady non-uniform currents. J Fluid Mech 10:529–549

MacIver RD, Simons RR, Thomas GP (2006) Gravity waves interacting with a narrow jet-like current. J Geophys Res 111:C03009

McLean JW, Ma YC, Martin DU, Saffman PG, Yuen HC (1981) Three-dimensional instability of finite-amplitude water waves. Phys Rev Lett 46:817–820

McLean JW (1982a) Instabilities of finite-amplitude gravity waves on water of finite depth. J Fluid Mech 114:331–341

McLean JW (1982b) Instabilities of finite-amplitude water waves. J Fluid Mech 114:315–330

Mei CC, Lo E (1984) The effects of a jet-like current on gravity waves in shallow water. J Phys Oceanogr 14:471–477

Onorato M, Proment D, Toffoli A (2011) Triggering rogue waves in opposing currents. Phys Rev Lett 107:184502

Peregrine DH (1976) Interaction of water waves and currents. Adv Appl Mech 16:9–117

Peregrine DH (1983) Breaking waves on beaches. Annu Rev Fluid Mech 15:149–178

Pullin DI, Grimshaw RHJ (1985) Stability of finite-amplitude interfacial waves, part 2, numerical results. J Fluid Mech 160:317–336

Pullin D, Grimshaw R (1986) Stability of finite-amplitude interfacial waves. Part 3. The effect of basic current shear for one-dimensional instabilities. J Fluid Mech 172:277–306

Ruban VP (2012) On the nonlinear schrödinger equation for waves on a nonuniform current. Jetp Lett 95:486–491

Senapati S, Kundu S, Debsarma S, Das KP (2016) Nonlinear evolution equations in crossing seas in the presence of uniform wind flow. Eur J Mech B/fluids 60:110–118

Stocker J, Peregrine DH (1999) The current-modified nonlinear schrödinger equation. J Fluid Mech 399:335–353

Toffoli A, Waseda T, Houtani H, Kinoshita T, Collins K, Proment D, Onorato M (2013) Excitation of rogue waves in a variable medium: An experimental study on the interaction of water waves and currents. Phys Rev E 87:051201

Toffoli A, Waseda T, Houtani H, Cavaleri L, Greaves D, Onorato M (2015) Rogue waves in opposing currents: An experimental study on deterministic and stochastic wave trains. J Fluid Mech 769:277–297

Turpin FM, Benmoussa C, Mei CC (1983) Effects of slowly varying depth and current on the evolution of a stokes wavepacket. J Fluid Mech 132:1–23

Whitham G (1967) Non-linear dispersion of water waves. J Fluid Mech 27(2):399–412

Yuen HC (1984) Nonlinear dynamics of in-terfacial waves. Physica D 12:71–82